Self-assembly of s-indacene-tetrone on Cu(111): molecular trapping and patterning of Cu adatoms

Nataliya Kalashnyk, Adam Hassan Denawi, Frédéric Dumur, Didier Gigmes, Xavier Bouju, Sylvain Clair

Self-assembly of *s*-indacene-tetrone on Cu(111): molecular trapping and patterning of Cu adatoms

Nataliya Kalashnyk[1], Adam Hassan Denawi[2], Frédéric Dumur[3], Didier Gigmes[3], Xavier Bouju[2,]*, Sylvain Clair[1,]*

[1] Aix-Marseille University, CNRS, IM2NP, Marseille, France.

[2] CEMES-CNRS, Université de Toulouse, 29 Rue J. Marvig, 31055 Toulouse, France.

[3] Aix-Marseille University, CNRS, ICR, Marseille France.

Abstract

The supramolecular self-assembly of *s*-indacene-1,3,5,7(2*H*,6*H*)-tetrone on the Cu(111) surface was investigated in ultrahigh vacuum by room-temperature scanning tunneling microscopy supported by theoretical modelling based on the density functional theory. In total, six different phases were found, driven by hydrogen bonding, metal ligand coordination or covalent coupling. Host-guest interactions allowed for the accommodation of molecular or metal clusters inside the open nanoporous patterns. In one phase, molecular trapping was stochastically observed inside the large periodic nanopores created inside the supramolecular network. The three metal-organic networks observed resulted in the creation of different kinds of regular arrays of isolated metal adatoms or adatom clusters with a lattice period larger than 1 nm.

Introduction

Supramolecular self-assembly of small planar aromatic molecules on well-defined surfaces is driven by the subtle balance between intermolecular bonding and molecule-substrate interactions.[1-7] While hydrogen bonds remain ubiquitous and largely dominating in many systems,[3-8] the formation of surface-supported metal-organic frameworks through complexation with metal adatoms[1,9-12] is particularly interesting because it represents an efficient approach for patterning a surface with a regular tessellation of isolated metal atoms with preserved properties for catalysis[13] or magnetism.[14-16] A wide range of different patterns, among the 17 wallpaper groups,[17] can be achieved by adequate control on the design of the organic precursor and on the growth conditions,[18] as revealed at the single molecule level by

scanning probe microscopy.[1-5] When supramolecular open networks are created on a surface, the 2D nanoporosity[5,19,20] can lead to particular confinement effects[21,22] such as the formation of quantum dots[23], host-guest molecular complexes,[24-27] or adatom trapping.[28-31]

In this article we show the formation of a variety of supramolecular networks based on hydrogen bonding or metal-organic complexation and exhibiting remarkable properties of molecular and adatom trapping. We have previously investigated extensively the molecule *s*-indacene-1,3,5,7(2*H*,6*H*)-tetrone ($INDO_4$, see inset in Fig. 1a)[32,33] on various silver surfaces.[27,34-36] This compound is formed of a small indacene backbone surrounded by four oxygen atoms with D2h symmetry and presents a remarkable ability to establish various intermolecular in-plane hydrogen bonds.[37] A variety of ordered phases can be obtained upon deposition of $INDO_4$ on silver surfaces, depending on the crystallographic orientation of the surface and on the growth conditions.[27,34-36] Motivated by the exceptional versatility of this precursor, we wanted to investigate its potential for creating metal-organic frameworks. The Cu(111) surface was chosen because it exhibits a large density of diffusing adatoms at room temperature and it represents a model substrate for creating coordination networks.[38-41] Similar to the case of silver surfaces, we observed the activation of covalent homocoupling at high annealing temperatures, but here exclusively based on the Knoevenagel reaction. The molecular precursors were deposited in ultrahigh vacuum (UHV) conditions and analyzed by room-temperature scanning tunneling microscopy (STM). Theoretical modeling is often necessary to interpret experimental results. Recently, a series of coarse-grained Monte Carlo simulations have been developed to interpret various two-dimensional molecular patterns,[42,43] especially for tetratomic molecules.[44-46] Here, numerical calculations based on the density functional theory (DFT) were performed to evidence the stability of the various coordination structures.

Results and discussion

Similarly to the case of $INDO_4$ deposited on Ag surfaces,[27,34-36] it is possible to form a large range of supramolecular networks upon adsorption of these molecules on Cu(111). Depending on the annealing temperature, we could identify six different phases, as reported in Table 1. At mild annealing temperature, the hydrogen-bonded phases KG1 and KG2 are formed while at higher annealing temperatures metal-organic self-assembly takes place in P3, P4 and P5 phases. At 470 K, a homo-coupling reaction is activated leading to the formation of a disordered covalent network (P6 phase). All STM experiments were performed at room temperature after the corresponding annealing procedures. A noisy background is systematically observed around the different molecular domains, thus revealing the presence of an additional molecular gas phase with high mobility.

	Phase	Annealing temperature [K]	Density [molecule.nm^{-2}]
H-bonded	KG1	RT	1.23
	KG2	350	1.17
Metal-organic	P3	390	1.14
	P4	430	1.18
	P5	430	0.80
Covalent network	P6	470	-/-

Table 1. Summary of the different phases observed for $INDO_4$ on Cu(111) in function of the annealing temperature. KG1 and KG2 are observed individually at the indicated annealing temperatures. For an annealing temperature of 430 K, all three metal-organic phases P3, P4 and P5 are observed co-existing on the surface. P6 is the only remaining phase above 470K.

Growth of H-bonded molecular networks

Upon deposition of $INDO_4$ derivative on the Cu(111) surface held at room temperature, we observe the growth of small ordered molecular islands (see Fig. 1a,b). A zoom-in STM image discloses the formation of the Kagome lattice KG1 composed of bright elongated protrusions whose dimensions match the size of the $INDO_4$ molecule. This structure is characterized by a large hexagonal network with a unit cell size of ~6.6 Å and comprising three molecules. A $\begin{pmatrix} 6 & 1 \\ -1 & 7 \end{pmatrix}$ superlattice unit cell can be determined for this molecular assembly, and evidences a purely epitaxial growth of the indacenes on the surface. The density of indacenes within this phase is thus reckoned at 1.23 molecules per nm^2. This phase exhibits chiral asymmetry and the opposite chirality was also observed (see Fig. S8).

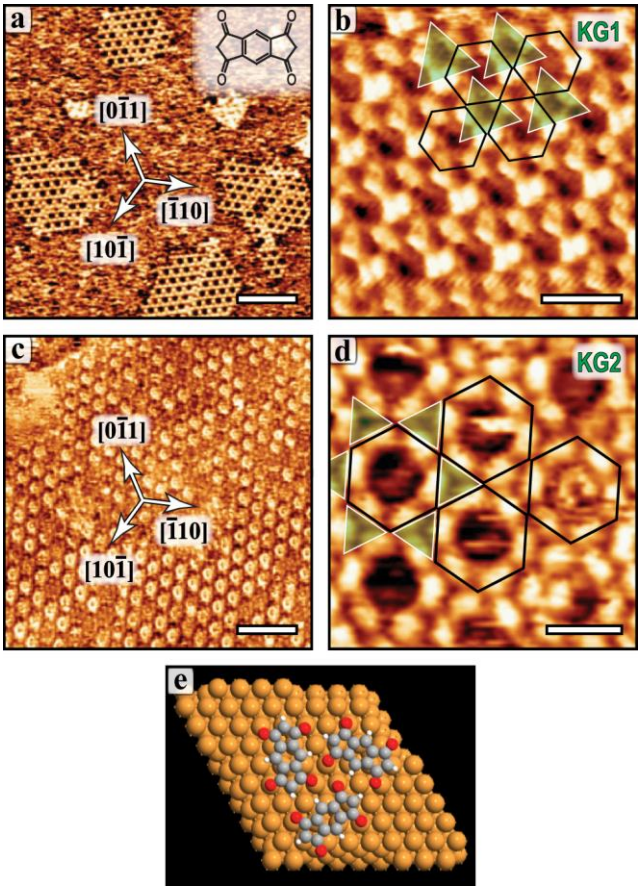

Figure 1. STM images of the hydrogen-bonded phases obtained upon deposition of $INDO_4$ (inset in (a)) on Cu(111) (a,b) at room temperature (KG1 phase) and (c,d) after annealing at 350 K (KG2 phase). Both phases are based on the same trimer motif modelled by DFT in (e) (see also Fig. S2). Scale bars: (a,c) 10 nm; (b,d) 2 nm.

Subsequent gentle annealing of the sample to a temperature of 350 K led to the growth of large islands exhibiting a novel supramolecular structure on the Cu(111) surface (see Fig. 1c,d). A close-up STM image shows the formation of another Kagome lattice (KG2) composed similarly of bright elongated protrusions with dimensions corresponding to that of the single molecule. This structure is characterized by a large hexagonal network with a unit cell size of 9.5 Å and comprising six molecules. A $\begin{pmatrix} 6 & 5 \\ -5 & 11 \end{pmatrix}$ superlattice unit cell can be determined for this phase, with a density of 1.17 molecules per nm^2.

Remarkably, in both KG1 and KG2 phases, the orientation of the long axis of indacene with respect to the $[1\bar{1}0]$-close packed directions of the Cu(111) substrate remains the same (i.e. ±25°, depending on the chiral orientation of the domain). These patterns are actually based on a single hydrogen-bonded unit, a molecular trimer arranged in triangular shape, that is organized either in a hexagonal lattice (in KG1) or

in a honeycomb lattice (in KG2). The intrinsic stability and structure of the hydrogen-bonded trimer was investigated by DFT calculations (see Fig. 1e and SI Fig. S2 for details). The triangle formed by the three inner oxygen atoms is almost isosceles (3.20 Å, 3.21 Å, 3.01 Å) whereas the three C-H···O hydrogen-bonds are characterized by (2.33 ± 0.09) Å and (151 ± 2)°. The partial Bader charges on each atom of the molecule do not differ from the case of a single adsorbed molecule (Fig. S1). In particular, the molecular axis is rotated by (36.8 ± 0.2)° with respect to the $[1\bar{1}0]$-direction.

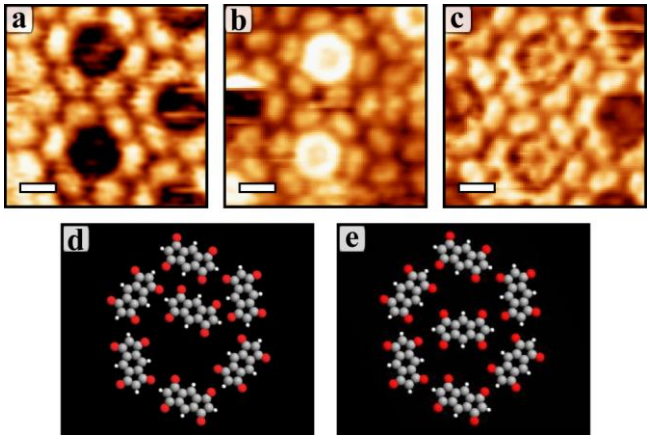

Figure 2. Zoomed-in STM images inside KG2 phase showing its nanoporosity (a) that is occasionally filled with a molecule in two different configurations (b,c). Scale bars: 1 nm. (d,e) DFT modelling of a single nanopore with a trapped molecule in lateral (d) or central position (e).

Although KG1 and KG2 structures have similar molecular densities (~1.2 nm^{-2}), the latter exhibits clearly large pores and can be regarded effectively as an open nanoporous network. By looking in closer details at the STM images of KG2 in Fig. 1c it is possible to observe an important number of defects appearing in the center of the pores of the network, as reported in Fig. 2. In fact, the pores are large enough to accommodate guest molecules. Because of the high symmetry of the pores, the guest may adopt different equivalent positions. As a result, the apparent STM contrast corresponds to the average occupation position, similar to other studies displaying dynamical systems.[27,47-49]

The molecular trapping inside a pore has been investigated by calculating the intermolecular interactions between the inside molecule and the six surrounding molecules forming a ring structure (Fig. 2d,e and Fig. S7). A more preferable configuration (see Table S2) is found for the inside molecule located in lateral position (Fig. 2d) closer to the molecules of the ring, indicating stronger attractive intermolecular interactions by hydrogen bonding as compared to the central position where van der Waals interactions are favored (Fig. 2e).

Formation of metal-organic frameworks

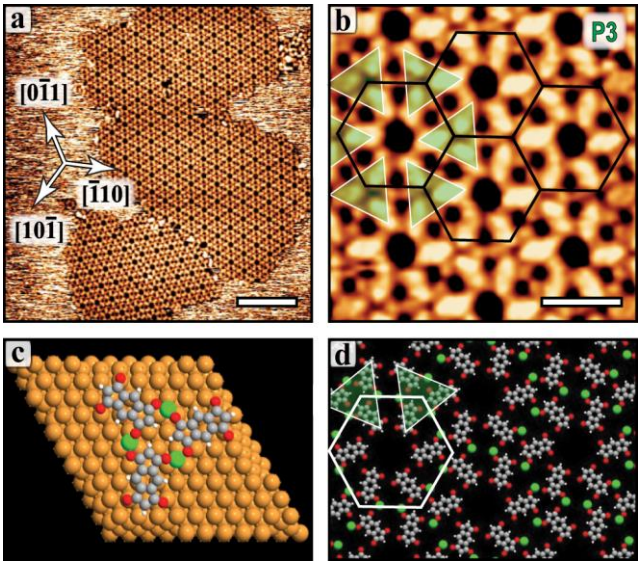

Figure 3. (a,b) STM images of the metal-organic phase P3 obtained upon deposition of $INDO_4$ on Cu(111) and annealing at 390 K. This phase is based on a trimer motif modelled by DFT in (c) (see also Fig. S3). (d) Configuration obtained from gas-phase DFT calculations. Scale bars: (a) 10 nm; (b) 2 nm.

Further increase of the annealing temperature to 390 K yields to the formation of a new chiral supramolecular phase with a hexagonal lattice (P3, see Fig. 3). A careful inspection of the high resolution STM images evidences the presence of not only elongated protrusions ascribed to the molecules but also of round shaped point-like features. The latter can be identified as Cu adatoms involved in a metal-organic phase. The high annealing temperature delivered an increased amount of intrinsic Cu adatoms that get coordinated by the organic precursors. The superstructure is characterized by a large hexagonal network with a unit cell size of 9.6 Å and comprising six molecules. A $\begin{pmatrix} 4 & 7 \\ -7 & 11 \end{pmatrix}$ superlattice unit cell can be determined for this phase, with a density of 1.14 molecules per nm^2. This phase again exhibits chiral asymmetry and the opposite chirality was also observed (see Fig. S9).

Similar to the previous KG1 and KG2 cases, a peculiar trimer motif can be identified as the basic bonding unit in P3 that is further organized in a honeycomb lattice. The intrinsic trimer here is of metal-organic nature and its stability and structure could be well reproduced by DFT calculations (see Fig. 3c and Fig. S3 for details). The copper adatoms are naturally located above hollow sites forming a triangle of (6.71 ± 0.05) Å, and are positioned below the mean plane generated by the molecular skeletons. The intermolecular interactions in the presence of the three adatoms generate the trimer with a Cu-O bond

equal to (2.00 ± 0.04) Å. Actually, there are two sets of distance, (1.96 ± 0.01) Å and (2.04 ± 0.01) Å, and the main distances between the surface plane and the six oxygen atoms close to the three Cu adatoms are (3.26 ± 0.01) Å and (2.90 ± 0.03) Å, respectively. This has to be compared with the *z*-position of the six other oxygen atoms, which is (2.27 ± 0.13) Å, indicating that the molecules do not stay flat above the surface in that case. The main molecular axis forms an angle with the Cu-Cu adatoms of (100.30 ± 0.05)° and of (29 ± 2)° with respect to $[1\bar{1}0]$-direction of the surface. Moreover, the three adatoms are positively charged (around -0.5 e^-, with $e^- = -|e| = -1.6 \times 10^{-19}$ C) due to the proximity of the oxygen atoms (~ +1.1 e^-) of the molecules. These results suggest that the structure is in rather strong interaction with the substrate. Indeed, the metal-organic interaction can be estimated as one order of magnitude larger than the hydrogen-bonding in this trimer structure (Fig. S5).

Furthermore, we could simulate a free-standing sheet of the metal-organic P3 network (Fig. 3d) based on the previous information. It should be noted here that, because the intrinsic adatoms can be sometimes difficult to evidence in STM images,[50,51] the proposed model that we have simulated may differ from the real network in terms of number and position of the metal adatoms. Nevertheless, our calculation shows that the reciprocal interaction between the molecules and the metal adatoms in this complex network is well equilibrated and can produce a robust and well-ordered organization.

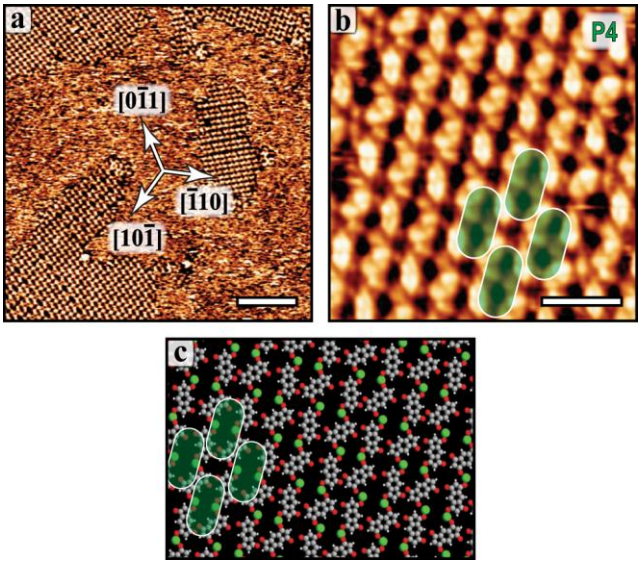

Figure 4. (a,b) STM images of the metal-organic phase P4 obtained upon deposition of $INDO_4$ on Cu(111) and annealing at 430 K and (c) corresponding model obtained from gas-phase DFT calculations. Scale bars: (a) 10 nm; (b) 2 nm.

Slight further annealing of the substrate from 390 K to 430 K leads to the formation of two additional anisotropic structures P4 and P5 dominating over the P3 one. For these novel phases, elongated and round shaped protrusions are visualized in the STM images indicating that both indacenes and Cu adatoms participate in the formation of these networks. The orientation of the molecules is the same as for the previous P3 structure. The P4 phase (Fig. 4) can be described with a rhombic unit cell (**a** = 5.0 Å, **b** = 5.3 Å, and ∠**a**, **b** = 79°) comprising two molecules. The P5 phase (Fig. 5) can be described with a quasi-rectangular unit cell (**a** = 12.1 Å, **b** = 7.9 Å, and ∠**a**, **b** = 87°) comprising five molecules. Consequently, the superlattice unit cells of these networks are found to be $\begin{pmatrix} 5 & 0 \\ -2 & 6 \end{pmatrix}$ and $\begin{pmatrix} 13 & -2 \\ -3 & 7 \end{pmatrix}$, with molecular densities of 1.18 nm^{-2} and 0.80 nm^{-2}, respectively. Phase P4 exhibits chiral asymmetry and it is found in six equivalent orientational domains (see Fig. S9 for P4). Phase P5 is more limited in its domain extension and exhibits a reduced order.

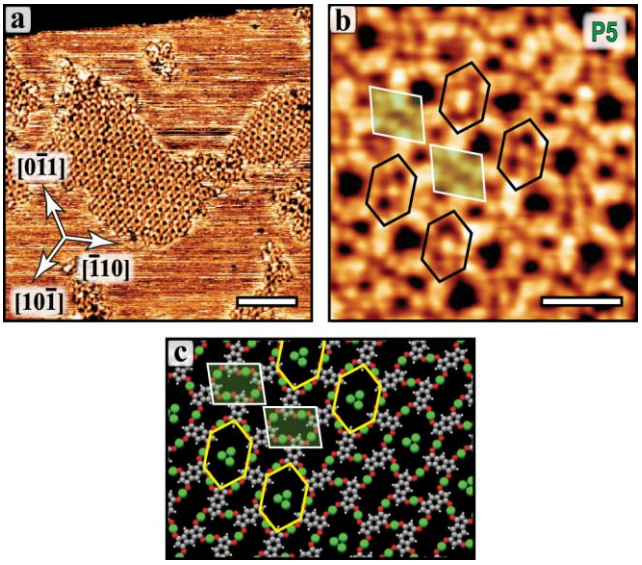

Figure 5. (a,b) STM images of the metal-organic phase P5 obtained upon deposition of $INDO_4$ on Cu(111) and annealing at 430 K and (c) the corresponding model obtained from gas-phase DFT calculations. Scale bars: (a) 10 nm; (b) 2 nm.

We could propose a model structure for the P4 (Fig. 4c) and P5 (Fig. 5c) phases in a free-standing configuration. For the P5 structure (Fig. 5c), we propose that adatom trimers are trapped inside the pores because the dimension of the latter is large enough to accommodate more than a single adatom (see also Fig. S6). However, because it is often impossible to distinguish between an isolated metal adatom and a small cluster in the STM images,[41,52,53] we cannot conclude unambiguously whether the center metal

structure is composed of a single adatom or an adatom trimer. In the P5 phase, the distances between the trapped metal adatoms and the ligand are remarkably large (the mean distance between the trimer barycenter and the six surrounding hydrogen atoms of the molecules is (5.8 ± 1.0) Å). Similar structures have been also previously observed, where adatoms were included inside quite large nanocavities formed by a supramolecular network.[28-31] In the present case, it has to be noted that the trapping of the adatoms is made possible thanks to a relatively important decrease of the molecular density of the network (see Table 1).

Formation of covalent structures

When the temperature is raised above 470 K the homocoupling reaction is taking place leading to a disordered covalent network (phase P6, Fig. 6). Remarkably here, only the Knoevenagel coupling is allowed and no oxidative coupling was observed, in opposition to the case of silver surfaces.[34,36,54] This is directly related to the fact that the Knoevenagel reaction is a less energy-demanding reaction than the oxidative coupling. Indeed, oxidative coupling can only be carried out in the presence of a metal catalyst in order to lower the energy barrier of the reaction.[55] In absence of metal catalyst, an insurmountable energy barrier exists so that the coupling reaction is unable to proceed. This is not the case for Knoevenagel reactions that can be carried out in metal-catalyst free conditions.[56] Typically, Knoevenagel reactions are catalyzed with a base and in this field, piperidine is a popular base. By using this base, theoretical calculations and experimental results revealed the free energy barrier of the reaction to be low, around 20.0 kcal/mol.[57] Additionally, based on the supramolecular phases P4/P5 obtained at lower temperatures, the orientations of the molecules are favorable so that the activated methylene groups of $INDO_4$ can directly react with the adjacent ketone functions. Indeed, the Knoevenagel reaction consists in a dehydrative coupling between a carbonyl group and an activated methylene group, what is achieved in $INDO_4$ with the presence of two electron-withdrawing ketone groups standing on both sides of the methylene group.

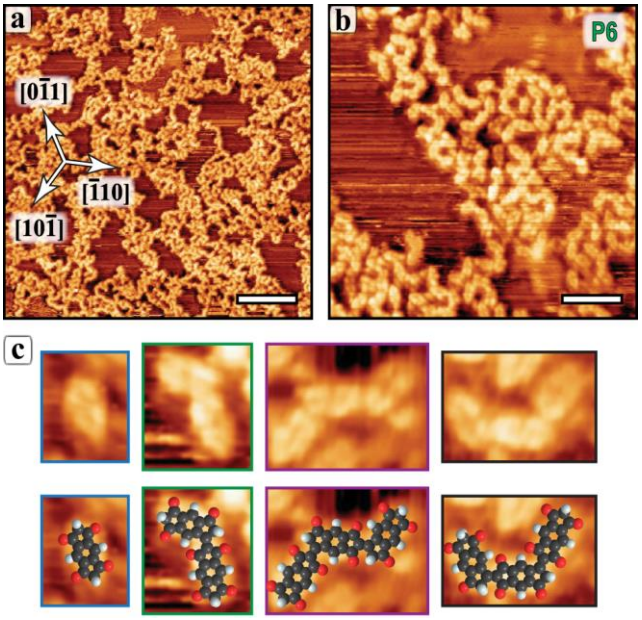

Figure 6. (a,b) STM images of the disordered covalent network P6 obtained upon deposition of $INDO_4$ on Cu(111) and annealing at 470 K. Scale bars: (a) 10 nm; (b) 3 nm. (c) High resolution STM images of the different molecular features observed inside the network and corresponding molecular models based on the Knoevenagel reaction.

Conclusions

For the system $INDO_4$/Cu(111) at room temperature, we have described the formation of six phases based on hydrogen bonding, metal ligand coordination or covalent coupling. Two Kagome networks were found, one of them with an important nanoporosity providing the ability to self-accommodate guest molecules.[27] Kagome supramolecular lattices are particularly attractive due to their specific topological electronic structure.[58-62] The different metal-organic phases P3, P4 and P5 represent well-defined robust self-organized patterns of metal adatoms, either directly involved in metal-organic bonds, or isolated and well-separated from the neighboring molecules. The complexity of the unit cells involving a large number of molecules and their relatively large sizes (up to 1 nm) can provide potentially interesting properties to such systems with regard to catalysis or magnetism.

Finally, for higher annealing temperature we observed the homocoupling of the precursor from the Knoevenagel reaction. The latter has only been scarcely reported on surfaces[34,63,64] and represents a promising approach for the formation of C=C bonds.

Methods

The DFT calculations were performed via the Vienna ab initio simulation package (VASP),[65] where the projector augmented wave (PAW) potential[66] was employed, while the exchange–correlation functional along with the generalized gradient approximation (GGA) by Perdew, Burke, and Ernzerhof (PBE)[67] was used. The 400 eV cut-off energy with the convergence criteria of 10^{-4} eV were set for the minimization. Only a single k-point, namely the Γ-point, was used for the calculations. The structure were relaxed until the residual forces were smaller than 0.02 eV/Å. Moreover, the van der Waals dispersion correction term of DFT-D3 method proposed by Grimme[68] was also adopted. The substrate is simulated by a 5-layers Cu(111) surface onto which we add the Cu-ITO molecules. The separation distance between the slabs, (top vacuum) is set to 20 Å.

The experiments were performed in ultra-high vacuum (UHV, base pressure in the low 10^{-10} mbar range). The single-crystal Cu(111) surface was cleaned by several cycles of Ar^+ bombardment followed by annealing. $INDO_4$ molecules were provided by Sigma-Aldrich as *rare and unique chemical*. The precursors were thoroughly degassed prior to deposition onto the atomically clean substrate held at room temperature (RT). The molecular powder was thermally sublimated from an evaporator heated to 150 °C for typical dosing time of 30 min providing coverage of ~0.5 monolayer. STM measurements were performed with a commercial Omicron VT-STM system operated at room temperature. The STM images were acquired in constant current mode with typical tunneling current $I_T \approx 0.3$ nA and sample bias $V_T \approx -(1–1.5)$ V. All images were subsequently calibrated using atomically resolved images of the pristine surfaces. Images were partly treated with the free softwares WSxM[69] and LMAPper.[70] An error bar of typically ± 1 Å is found for each distance measurement in the STM images. The proposed superstructure matrices are derived from the measured unit cell sizes and the symmetry considerations of each phase corresponding to the observation of the different symmetry-equivalent domains.

Acknowledgments

HD and XB mention that this study has been supported through the EUR grant NanoX n°ANR-17-EURE-0009 in the framework of the "Programme des Investissements d'Avenir". This work was granted access to the HPC resources of CALMIP supercomputing center under the allocation 2021-P0832.

References

(1) Dong, L.; Gao, Z. A.; Lin, N. Self-assembly of metal-organic coordination structures on surfaces. *Prog. Surf. Sci.* **2016,** *91*, 101-135.

(2) Clair, S.; De Oteyza, D. G. Controlling a Chemical Coupling Reaction on a Surface: Tools and Strategies for On-Surface Synthesis. *Chem. Rev.* **2019,** *119*, 4717-4776.

(3) Brown, R. D.; Corcelli, S. A.; Kandel, S. A. Structural Polymorphism as the Result of Kinetically Controlled Self-Assembly. *Acc. Chem. Res.* **2018,** *51*, 465-474.

(4) Barth, J. V. Molecular Architectonic on Metal Surfaces. *Annu. Rev. Phys. Chem.* **2007,** *58*, 375-407.

(5) Kudernac, T.; Lei, S. B.; Elemans, J.; De Feyter, S. Two-dimensional supramolecular self-assembly: nanoporous networks on surfaces. *Chem. Soc. Rev.* **2009,** *38*, 402-421.

(6) Bouju, X.; Mattioli, C.; Franc, G.; Pujol, A.; Gourdon, A. Bicomponent Supramolecular Architectures at the Vacuum-Solid Interface. *Chem. Rev.* **2017,** *117*, 1407-1444.

(7) Clair, S.; Pons, S.; Seitsonen, A. P.; Brune, H.; Kern, K.; Barth, J. V. STM Study of Terephthalic Acid Self-Assembly on Au(111): Hydrogen-Bonded Sheets on an Inhomogeneous Substrate. *J. Phys. Chem. B* **2004,** *108*, 14585-14590.

(8) Yu, M.; Kalashnyk, N.; Barattin, R.; Benjalal, Y.; Hliwa, M.; Bouju, X.; Gourdon, A.; Joachim, C.; Laegsgaard, E.; Besenbacher, F.; et al. Self-assembly of hydrogen-bonded chains of molecular landers. *Chem. Commun.* **2010,** *46*, 5545-5547.

(9) Barth, J. V. Fresh Perspectives for Surface Coordination Chemistry. *Surf. Sci.* **2009,** *603*, 1533-1541.

(10) Lin, N.; Stepanow, S.; Ruben, M.; Barth, J. V. In *Templates in Chemistry Iii*; Springer-Verlag Berlin: Berlin, 2009; Vol. 287; p 1-44.

(11) Liu, J.; Abel, M.; Lin, N. On-Surface Synthesis: A New Route Realizing Single-Layer Conjugated Metal-Organic Structures. *J. Phys. Chem. Lett.* **2022,** *13*, 1356-1365.

(12) Ashworth, D. J.; Foster, J. A. Metal-organic framework nanosheets (MONs): a new dimension in materials chemistry. *J. Mater. Chem. A* **2018,** *6*, 16292-16307.

(13) Grumelli, D.; Wurster, B.; Stepanow, S.; Kern, K. Bio-inspired nanocatalysts for the oxygen reduction reaction. *Nat. Commun.* **2013,** *4*, 2904.

(14) Gambardella, P.; Stepanow, S.; Dmitriev, A.; Honolka, J.; de Groot, F. M. F.; Lingenfelder, M.; Sen Gupta, S.; Sarma, D. D.; Bencok, P.; Stanescu, S.; et al. Supramolecular Control of the Magnetic Anisotropy in Two-Dimensional High-Spin Fe Arrays at a Metal Interface. *Nat. Mater.* **2009,** *8*, 189-193.

(15) Giovanelli, L.; Savoyant, A.; Abel, M.; Maccherozzi, F.; Ksari, Y.; Koudia, M.; Hayn, R.; Choueikani, F.; Otero, E.; Ohresser, P.; et al. Magnetic Coupling and Single-Ion Anisotropy in Surface-Supported Mn-Based Metal-Organic Networks. *J. Phys. Chem. C* **2014,** *118*, 11738-11744.

(16) Xie, L.; Lin, H. P.; Zhang, C.; Li, J. C.; Merino-Diez, N.; Friedrich, N.; Bouju, X.; Li, Y. Y.; Pascual, J. I.; Xu, W. Switching the Spin on a Ni Trimer within a Metal-Organic Motif by Controlling the On-Top Bromine Atom. *ACS Nano* **2019,** *13*, 9936-9943.

(17) Liu, L.; Choi, G. P. T.; Mahadevan, L. Wallpaper group kirigami. *Proceedings of the Royal Society a-Mathematical Physical and Engineering Sciences* **2021,** *477*, 20210161.

(18) Stepanow, S.; Lingenfelder, M.; Dmitriev, A.; Spillmann, H.; Delvigne, E.; Lin, N.; Deng, X.; Cai, C.; Barth, J. V.; Kern, K. Steering Molecular Organization and Host-Guest Interactions using Tailor-Made Two-Dimensional Nanoporous Coordination Systems. *Nat. Mater.* **2004,** *3*, 229.

(19) Jasper-Tonnies, T.; Gruber, M.; Ulrich, S.; Herges, R.; Berndt, R. Coverage-Controlled Superstructures of C-3-Symmetric Molecules: Honeycomb versus Hexagonal Tiling. *Angew. Chem. Int. Ed.* **2020,** *59*, 7008-7017.

(20) Zhang, L.; Zou, B.; Dong, D.; Huo, F. W.; Zhang, X.; Chi, L. F.; Jiang, L. Self-assembled monolayers of new dendron-thiols: manipulation of the patterned surface and wetting properties. *Chem. Commun.* **2001,** *19*, 1906-1907.

(21) Muller, K.; Enache, M.; Stöhr, M. Confinement properties of 2D porous molecular networks on metal surfaces. *J. Phys. Condens. Matter.* **2016,** *28*, 153003.

(22) Kumar, A.; Banerjee, K.; Foster, A. S.; Liljeroth, P. Two-Dimensional Band Structure in Honeycomb Metal Organic Frameworks. *Nano Lett.* **2018,** *18*, 5596-5602.

(23) Piquero-Zulaica, I.; Lobo-Checa, J.; Sadeghi, A.; Abd El-Fattah, Z. M.; Mitsui, C.; Okamoto, T.; Pawlak, R.; Meier, T.; Arnau, A.; Ortega, J. E.; et al. Precise engineering of quantum dot array coupling through their barrier widths. *Nat. Commun.* **2017,** *8*, 6.

(24) Khan, S. B.; Lee, S. L. Supramolecular Chemistry: Host-Guest Molecular Complexes. *Molecules* **2021,** *26*, 3995.

(25) Cui, D.; MacLeod, J. M.; Ebrahimi, M.; Perepichka, D. F.; Rosei, F. Solution and Air Stable Host/Guest Architectures from a Single Layer Covalent Organic Framework. *Chem. Commun.* **2015,** *51*, 16510-16513.

(26) Stöhr, M.; Wahl, M.; Spillmann, H.; Gade, L. H.; Jung, T. A. Lateral manipulation for the positioning of molecular guests within the confinements of a highly stable self-assembled organic surface network. *Small* **2007,** *3*, 1336-1340.

(27) Kalashnyk, N.; Clair, S. Self-Accommodating Honeycomb Networks from Supramolecular Self-Assembly of s-Indacene-tetrone on Silver Surfaces. *Langmuir* **2022,** *38*, 1067-1071.

(28) Schiffrin, A.; Reichert, J.; Auwarter, W.; Jahnz, G.; Pennec, Y.; Weber-Bargioni, A.; Stepanyuk, V. S.; Niebergall, L.; Bruno, P.; Barth, J. V. Self-aligning atomic strings in surface-supported biomolecular gratings. *Phys. Rev. B* **2008,** *78*, 035424.

(29) Zhang, Y. Q.; Paszkiewicz, M.; Du, P.; Zhang, L. D.; Lin, T.; Chen, Z.; Klyatskaya, S.; Ruben, M.; Seitsonen, A. P.; Barth, J. V.; et al. Complex Supramolecular Interfacial Tessellation through Convergent Multi-Step Reaction of a Dissymmetric Simple Organic Precursor. *Nat. Chem.* **2018,** *10*, 296-304.

(30) Pivetta, M.; Pacchioni, G. E.; Schlickum, U.; Barth, J. V.; Brune, H. Formation of Fe Cluster Superlattice in a Metal-Organic Quantum-Box Network. *Phys. Rev. Lett.* **2013,** *110*, 086102.

(31) Zhang, W. Z.; Wang, T.; Han, D.; Huang, J. M.; Feng, L.; Ding, H. H.; Hu, J.; Zeng, Z. W.; Xu, Q.; Zhu, J. F. Stepwise Synthesis of N-Ag-N and C-Ag-C Organometallic Structures on a Ag(111) Surface. *J. Phys. Chem. C* **2020,** *124*, 16415-16422.

(32) Krief, P.; Becker, J. Y.; Ellern, A.; Khodorkovsky, V.; Neilands, O.; Shapiro, L. s-indacene-1,3,5,7(2H,6H)-tetraone ('Janus dione') and 1,3-dioxo-5,6-indane-dicarboxylic acid: Old and new 1,3-indandione derivatives. *Synthesis-Stuttgart* **2004,** *15*, 2509-2512.

(33) Sprick, R. S.; Thomas, A.; Scherf, U. Acid catalyzed synthesis of carbonyl-functionalized microporous ladder polymers with high surface area. *Polymer Chemistry* **2010,** *1*, 283-285.

(34) Kalashnyk, N.; Salomon, E.; Mun, S. H.; Jung, J.; Giovanelli, L.; Angot, T.; Dumur, F.; Gigmes, D.; Clair, S. The Orientation of Silver Surfaces Drives the Reactivity and the Selectivity in Homo‐Coupling Reactions. *ChemPhysChem* **2018,** *19*, 1802-1808.

(35) Kalashnyk, N.; Dumur, F.; Gigmes, D.; Clair, S. Molecular adaptation in supramolecular self-assembly: brickwall-type phases of indacene-tetrone on silver surfaces. *Chem. Commun.* **2018,** *54*, 8510-8513.

(36) Kalashnyk, N.; Mouhat, K.; Oh, J.; Jung, J.; Xie, Y.; Salomon, E.; Angot, T.; Dumur, F.; Gigmes, D.; Clair, S. On-Surface Synthesis of Aligned Functional Nanoribbons Monitored by Scanning Tunneling Microscopy and Vibrational Spectroscopy. *Nat. Commun.* **2017,** *8*, 14735.

(37) Sigalov, M.; Krief, P.; Shapiro, L.; Khodorkovsky, V. Inter- and intramolecular C-H...O bonding in the anions of 1,3-indandione derivatives. *Eur. J. Org. Chem.* **2008,** *4*, 673-683.

(38) Lin, N.; Dmitriev, A.; Weckesser, J.; Barth, J. V.; Kern, K. Real-time single-molecule imaging of the formation and dynamics of coordination compounds. *Angew. Chem. Int. Ed.* **2002,** *41*, 4779-4783.

(39) Faraggi, M. N.; Rogero, C.; Arnau, A.; Trelka, M.; Ecija, D.; Isvoranu, C.; Schnadt, J.; Marti-Gastaldo, C.; Coronado, E.; Gallego, J. M.; et al. Role of Deprotonation and Cu Adatom Migration in Determining the Reaction Pathways of Oxalic Acid Adsorption on Cu(111). *J. Phys. Chem. C* **2011,** *115*, 21177-21182.

(40) Kunkel, D. A.; Hooper, J.; Simpson, S.; Beniwal, S.; Morrow, K. L.; Smith, D. C.; Cousins, K.; Ducharme, S.; Zurek, E.; Enders, A. Rhodizonic Acid on Noble Metals: Surface Reactivity and Coordination Chemistry. *J. Phys. Chem. Lett.* **2013,** *4*, 3413-3419.

(41) Bebensee, F.; Svane, K.; Bombis, C.; Masini, F.; Klyatskaya, S.; Besenbacher, F.; Ruben, M.; Hammer, B.; Linderoth, T. R. A Surface Coordination Network Based on Copper Adatom Trimers. *Angew. Chem. Int. Ed.* **2014,** *53*, 12955-12959.

(42) Nieckarz, D.; Szabelski, P. Understanding Pattern Formation in 2D Metal-Organic Coordination Systems on Solid Surfaces. *J. Phys. Chem. C* **2013,** *117*, 11229-11241.

(43) Gdula, K.; Nieckarz, D. On-Surface Self-Assembly of Metal-Organic Architectures: Insights from Computer Simulations. *J. Phys. Chem. C* **2020,** *124*, 20066-20078.

(44) Bischoff, F.; He, Y. Q.; Seufert, K.; Stassen, D.; Bonifazi, D.; Barth, J. V.; Auwarter, W. Tailoring Large Pores of Porphyrin Networks on Ag(111) by MetalOrganic Coordination. *Chem. Eur. J.* **2016,** *22*, 15298-15306.

(45) Nieckarz, D.; Rzysko, W.; Szabelski, P. On-surface self-assembly of tetratopic molecular building blocks. *Phys. Chem. Chem. Phys.* **2018,** *20*, 23363-23377.

(46) Nieckarz, D.; Szabelski, P. Surface-Confined Self-Assembly of Asymmetric Tetratopic Molecular Building Blocks. *ChemPhysChem* **2019,** *20*, 1850-1859.

(47) Palma, C. A.; Bjork, J.; Rao, F.; Kuhne, D.; Klappenberger, F.; Barth, J. V. Topological Dynamics in Supramolecular Rotors. *Nano Lett.* **2014,** *14*, 4461-4468.

(48) Palma, C. A.; Bjork, J.; Klappenberger, F.; Arras, E.; Kuhne, D.; Stafstrom, S.; Barth, J. V. Visualization and thermodynamic encoding of single-molecule partition function projections. *Nat. Commun.* **2015,** *6*, 6210.

(49) Karamzadeh, B.; Eaton, T.; Torres, D. M.; Cebula, I.; Mayor, M.; Buck, M. Sequential nested assembly at the liquid/solid interface. *Faraday Discuss.* **2017,** *204*, 173-190.

(50) Blowey, P. J.; Velari, S.; Rochford, L. A.; Duncan, D. A.; Warr, D. A.; Lee, T. L.; De Vita, A.; Costantini, G.; Woodruff, D. P. Re-evaluating how charge transfer modifies the conformation of adsorbed molecules. *Nanoscale* **2018,** *10*, 14984-14992.

(51) Ryan, P.; Blowey, P. J.; Sohail, B. S.; Rochford, L. A.; Duncan, D. A.; Lee, T.-L.; Starrs, P.; Costantini, G.; Maurer, R. J.; Woodruff, D. P. Thermodynamic Driving Forces for Substrate Atom Extraction by Adsorption of Strong Electron Acceptor Molecules. *The Journal of Physical Chemistry C* **2022,** *126*, 6082-6090.

(52) Rochefort, A.; Vernisse, L.; Gomez-Herrero, A. C.; Sanchez-Sanchez, C.; Martin-Gago, J. A.; Cherioux, F.; Clair, S.; Coraux, J.; Martinez, J. I. Role of the Structure and Reactivity of Cu and Ag Surfaces in the Formation of a 2D Metal-Hexahydroxytriphenylene Network. *J. Phys. Chem. C* **2021,** *125*, 17333-17341.

(53) Zhang, C.; Kazuma, E.; Kim, Y. Atomic-Scale Visualization of the Stepwise Metal-Mediated Dehalogenative Cycloaddition Reaction Pathways: Competition between Radicals and Organometallic Intermediates. *Angew. Chem. Int. Ed.* **2019,** *58*, 17736-17744.

(54) Hussein, F.; Pigot, C.; Romero-Lairado, F.; Minissale, M.; Salomon, E.; Angot, T.; Dumur, F.; Nechab, M.; Gigmes, D.; Clair, S.; et al. On-surface homocoupling reactivity of a chiral bifunctional bromoindanone molecule on Cu(111). *New J. Chem.* **2022,** *46*, 22869-22876.

(55) Funes-Ardoiz, I.; Maseras, F. Oxidative Coupling Mechanisms: Current State of Understanding. *Acs Catalysis* **2018,** *8*, 1161-1172.

(56) Dalessandro, E. V.; Collin, H. P.; Valle, M. S.; Pliego, J. R. Mechanism and free energy profile of base-catalyzed Knoevenagel condensation reaction. *RSC Adv.* **2016,** *6*, 57803-57810.

(57) Dalessandro, E. V.; Collin, H. P.; Guimaraes, L. G. L.; Valle, M. S.; Pliego, J. R. Mechanism of the Piperidine-Catalyzed Knoevenagel Condensation Reaction in Methanol: The Role of Iminium and Enolate Ions. *J. Phys. Chem. B* **2017,** *121*, 5300-5307.

(58) Hua, M.; Xia, B.; Wang, M.; Li, E.; Liu, J.; Wu, T.; Wang, Y.; Li, R.; Ding, H.; Hu, J.; et al. Highly Degenerate Ground States in a Frustrated Antiferromagnetic Kagome Lattice in a Two-Dimensional Metal–Organic Framework. *The Journal of Physical Chemistry Letters* **2021,** *12*, 3733-3739.

(59) Hernandez-Lopez, L.; Piquero-Zulaica, I.; Downing, C. A.; Piantek, M.; Fujii, J.; Serrate, D.; Ortega, J. E.; Bartolome, F.; Lobo-Checa, J. Searching for kagome multi-bands and edge states in a predicted organic topological insulator. *Nanoscale* **2021,** *13*, 5216-5223.

(60) Anindya, K. N.; Rochefort, A. Controlling the magnetic properties of two-dimensional carbon-based Kagome polymers. *Carbon Trends* **2022,** *7*, 100170.

(61) Pawlak, R.; Liu, X. S.; Ninova, S.; D'Astolfo, P.; Drechsel, C.; Liu, J. C.; Haner, R.; Decurtins, S.; Aschauer, U.; Liu, S. X.; et al. On-Surface Synthesis of Nitrogen-Doped Kagome Graphene. *Angew. Chem. Int. Ed.* **2021,** *60*, 8370-8375.

(62) Kumar, D.; Hellerstedt, J.; Field, B.; Lowe, B.; Yin, Y. F.; Medhekar, N. V.; Schiffrin, A. Manifestation of Strongly Correlated Electrons in a 2D Kagome Metal-Organic Framework. *Adv. Funct. Mater.* **2021,** *31*, 2106474.

(63) Au-Yeung, K. H.; Kuhne, T.; Becker, D.; Richter, M.; Ryndyk, D. A.; Cuniberti, G.; Heine, T.; Feng, X. L.; Moresco, F. On-Surface Formation of Cyano-Vinylene Linked Chains by Knoevenagel Condensation. *Chem. Eur. J.* **2021,** *27*, 17336-17340.

(64) Geng, Y. F.; Dai, H. L.; Chang, S. Q.; Hu, F. Y.; Zeng, Q. D.; Wang, C. Formation of C=C Bond via Knoevenagel Reaction between Aromatic Aldehyde and Barbituric Acid at Liquid/HOPG and Vapor/HOPG Interfaces. *ACS Appl. Mater. Interfaces* **2015,** *7*, 4659-4666.

(65) Kresse, G.; Joubert, D. From ultrasoft pseudopotentials to the projector augmented-wave method. *Phys. Rev. B* **1999,** *59*, 1758-1775.

(66) Blöchl, P. E. Projector augmented-wave method. *Phys. Rev. B* **1994,** *50*, 17953-17979.

(67) Perdew, J. P.; Burke, K.; Ernzerhof, M. Generalized gradient approximation made simple. *Phys. Rev. Lett.* **1996,** *77*, 3865-3868.

(68) Grimme, S.; Antony, J.; Ehrlich, S.; Krieg, H. A consistent and accurate ab initio parametrization of density functional dispersion correction (DFT-D) for the 94 elements H-Pu. *J. Chem. Phys.* **2010,** *132*, 154104.

(69) Horcas, I.; Fernández, R.; Gómez-Rodríguez, J. M.; Colchero, J.; Gómez-Herrero, J.; Baro, A. M. WSXM: A software for scanning probe microscopy and a tool for nanotechnology. *Rev. Sci. Inst.* **2007,** *78*, 013705.

(70) https://sourceforge.net/projects/spm-and-mol-viewer/.